IOP PUBLISHING NANOTECHNOLOGY
Nanotechnology **18** (2007) 175103 (5pp) doi:10.1088/0957-4484/18/17/175103

In vivo SPECT/CT imaging and biodistribution using radioactive $Cd^{125m}Te/ZnS$ nanoparticles

Jonathan D Woodward[1], Steve J Kennel[2], Saed Mirzadeh[3], Sheng Dai[1], Jonathan S Wall[2], Tina Richey[2], James Avenell[2] and Adam J Rondinone[1,4]

[1] Chemical Sciences Division and Center for Nanophase Materials Sciences, Oak Ridge National Laboratory, USA
[2] University of Tennessee Health Science Center, College of Medicine, Knoxville, USA
[3] Nuclear Science and Technology Division, Oak Ridge National Laboratory, USA

Received 16 January 2007, in final form 16 February 2007
Published 2 April 2007
Online at stacks.iop.org/Nano/18/175103

Abstract
Radioactive cadmium telluride/zinc sulfide ($Cd^{125m}Te/ZnS$) nanoparticles were targeted to mouse lung with antibody to mouse lung endothelium and quantified using radiological histology in order to test the *in vivo* targeting efficacy of a nanoparticle–antibody (NP–mAb) system. The nanoparticles were linked to either a monoclonal antibody to mouse lung thrombomodulin (mAb 201B) or a control antibody (mAb 33), and injected into groups of 6-week-old Balb/C female mice. Animals were sacrificed at 1, 4, 24, 72 and 144 h post-injection, and biodistribution in major organs was determined. Full body microSPECT/CT imaging was performed on a pair of mice (experimental and control) providing visual confirmation of the biodistribution. The $Cd^{125m}Te/ZnS$ NPs conjugated to mAb 201B principally target the lungs while the nanoparticles coupled to mAb 33 accumulate in the liver and spleen. These data provide, for the first time, a quantitative measurement of the *in vivo* targeting efficacy of an inorganic nanoparticle–mAb system.

S Supplementary data are available from stacks.iop.org/Nano/18/175103

M This article features online multimedia enhancements

Nanoparticles (NP) of various materials have been coupled to antibodies and the resulting conjugates may find application as targeted drug delivery systems or diagnostic tools in medical imaging [1–7]. Similarly, radionuclides with specific emission properties may be incorporated into metal–chalcogenide and metal–oxide NPs, and when bound to targeting antibodies may become targeted radioisotope delivery systems for radioimmunotherapy and radioimaging. The nanoparticle–antibody conjugates (NP–mAb) may be injected into the bloodstream to target non-solid tumours or accessible sites in tumour blood vessels for beta and alpha therapy or for single photon emission computed tomography (SPECT) and positron emission tomography (PET) imaging. Conventional radioimmunotherapies have utilized molecular radionuclide chelators ($^{90}Y(\beta^-)$, Zevalin™) or direct iodination ($^{131}I(\beta^- + \gamma)$, Bexxar™) of the targeting antibody (for a review see Goldenberg [8]). A NP-based alpha or beta radiotherapy may mitigate unintentional radiotoxic effects by effectively sequestering the radionuclides and their decay daughters, which is necessary when employing nanogenerator [9, 10] or *in vivo* generator radioisotopes [11, 12]. To date, there have been no reports on the quantitative biodistribution of inorganic radioisotope-containing NP–protein conjugates targeted to specific tissue *in vivo*. For the study of the biodistribution of nanoparticles that are of a significant mass compared to the targeting antibody, the most important question is targeting efficacy. The work reported here utilizes a well-characterized antibody system (mAb 201B to thrombomodulin [13]) coupled to radioactive NP ($Cd^{125m}Te/ZnS$) to measure the targeting efficacy of a NP-based therapy and the subsequent whole body

[4] Author to whom any correspondence should be addressed.

 © 2007 IOP Publishing Ltd Printed in the UK

biodistribution of the NP–mAb conjugates. Biodistribution performed through radiolabelling is inherently quantitative and is not subject to signal attenuation by the subject.

The CdTe/ZnS nanoparticles are well known for their fluorescent properties, and *in vivo* and *ex vivo* fluorescence imaging studies have been reported. While toxicity questions are likely to prevent CdTe/ZnS systems from being used clinically, the CdTe/ZnS system serves as a useful surrogate for answering questions about targeting efficacy. The CdSe/ZnS system was chosen because the techniques for synthesizing these nanoparticles are well developed, and the surfaces can be modified easily to facilitate protein coupling. Furthermore, the CdTe NPs can be doped with the radioisotope ^{125m}Te ($t_{1/2}$ = 58 days) which emits low-energy x- and γ-rays (27–30 and 35.5 keV, respectively) allowing for accurate verification of mAb performance and NP fate within the mouse. Gamma-emitting radionuclides are exceptional for biodistribution studies because the gamma-emitting nanoparticle can be detected anywhere in the mouse, allowing quantitative determination of targeting efficacy. The Cd^{125m}Te cores were capped with non-radioactive ZnS to prevent particle degradation in the mouse and leaching of ^{125m}Te into the bloodstream. Ultimately, a radioactive NP–mAb system could serve to deliver other diagnostic or therapeutic radioisotopes within the CdTe matrix. In that sense, the nanoparticle serves the purpose of a chelator. Primarily, the CdTe/ZnS nanoparticle serves as a validation model to evaluate the feasibility of employing other NPs (such as metal oxides) as drug or radioisotope delivery systems.

Cd^{125m}Te NPs were prepared based on the method of Peng [14], with the addition of a coating of zinc sulfide to cap the particles (see Experimental in supporting information available at stacks.iop.org/Nano/18/175103). In these experiments, highly enriched ^{124}Te containing radioactive ^{125m}Te was used rather than natural Te, and the batch size was reduced to produce 2 mg of nanoparticles. Te-125m is chemically identical to natural Te and does not alter the chemistry of any of the reactions. Instrumental analysis (NMR, TEM) was performed on non-radioactive particles synthesized under identical conditions using identical glassware, chemicals and batch size to characterize the NP size, morphology and surface chemistry. Synthesis of the radioactive nanoparticles took place in a designated radiological laboratory outfitted with a Schlenk line, HEPA hood and other ancillary equipment, using the necessary radiological controls (scrubs, dosimetry). In order to couple the Cd^{125m}Te/ZnS NPs to the mAb, the surfaces were derivatized with mercaptoacetic acid [1]. Although multiple options are available for conjugating NP to mAb, we chose the mercaptoacetic acid approach because it is simple to perform under difficult radiological conditions and results in the smallest nanoparticle–mAb conjugates.

The surface derivatized Cd^{125m}Te/ZnS NPs were reacted with either the targeting mAb (rat mAb 201B to murine thrombomodulin [15, 16]) or a non-reactive isotype-matched control antibody, mAb 33, using traditional carbodiimide based coupling chemistry [2]. The antibody to thrombomodulin was chosen because it reacts with a target antigen in the lumen of blood vessels and has been shown to accumulate rapidly and specifically in mouse lung [16]. After the coupling reaction, NP–mAb conjugates were purified from aggregated material and free mAb by gel filtration. A set of identical, non-radioactive NP–mAb samples was imaged using transmission electron microscopy (TEM; supplementary figure 1, available at stacks.iop.org/Nano/18/175103) immediately after gel chromatography. SDS-PAGE was used to characterize the radioactive fractions. Reduced (mercaptoethanol) and non-reduced samples of the radioactive mAb-NP conjugate were run on SDS-PAGE to verify that the nanoparticle was bound to the antibody (supplementary figure 2, available at stacks.iop.org/Nano/18/175103). The fraction containing molecules with an average molecular weight of approximately 1–5 $\times$ 10^6 Da, containing both mAb and Cd^{125m}Te/ZnS, was injected into two groups of Balb/c female mice. The first experimental group consisted of 25 mice sacrificed in groups of five at 1, 4, 24, 72 and 144 h post-injection. The second group, serving as a control, consisted of 10 mice which were sacrificed in groups of five at 1 and 24 h post-injection. Biodistribution analysis was performed using standard methods [13]. The radioactivity in the liver, spleen, kidney, lung and blood was measured and the per cent injected dose per gram of tissue (%ID/g, to normalize between organs) calculated. The four major organs plus blood accounted for approximately 85% of the injected radioactivity in each mouse. Also for comparison, unconjugated nanoparticles (lacking antibody) were tested for biodistribution in one pair of mice.

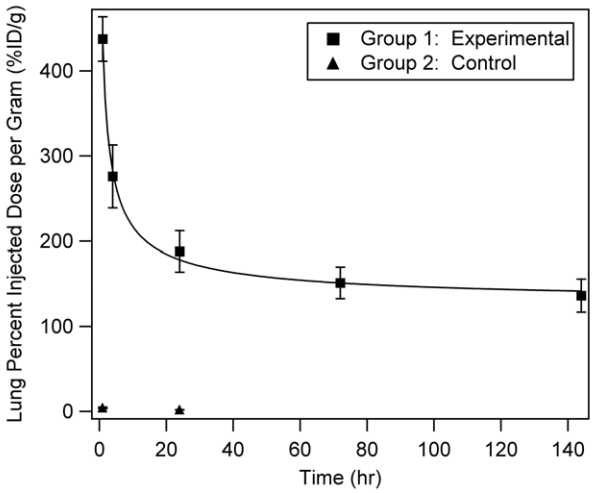

Figure 1. Group 1 mice, in which nanoparticles were linked to mAb 201B to murine thrombomodulin experience a 100-fold increase in radioactivity in the targeted organ (lung) over group 2 mice with NP coupled to control mAb33. Error bars = $\pm\sigma$. The initial radioactivity in the lung dropped quickly due to reduction of the S–S bond at some of the mercaptoacetic acid surface binding sites. Retained radioactivity was likely bond through less reactive S–Zn bonds.

Lung accumulation of targeted antibodies for both of these groups is shown in figure 1. Maximum accumulation (at 1 h) for group 1 that received the mAb 201B was 437 $\pm$ 26%ID/g tissue (a whole murine lung weighs $\sim$0.1 g) versus 4 $\pm$ 0.9%ID/g for the control animals of group 2. At 1 h, this represented a 100-fold increase in targeting efficacy versus control. The measured radioactivity for group 1 dropped rapidly within the first 24 h, levelling off at approximately 135%ID/g at 144 h (determined by fit using the Hill equation). After 6 days, the amount of radioactivity retained in the group

Table 1. Biodistribution of lung-targeted and untargeted control NP–mAb conjugates in 6-week-old Balb/C female mice, sacrificed in groups of five at designated intervals.

Post-injection period (h)	Lung	Spleen	Liver	Kidney	Blood
			Experimental %ID/g		
1	437 ± 26	15.3 ± 2.1	16.1 ± 1.0	11.9 ± 0.6	2.6 ± 0.5
4	276 ± 37	54.7 ± 7.9	25.0 ± 2.3	15.2 ± 1.7	2.1 ± 0.2
24	188 ± 24	66.1 ± 9.2	22.9 ± 2.7	17.3 ± 2.7	1.0 ± 0.2
72	151 ± 18	46.6 ± 8.3	18.4 ± 1.7	15.1 ± 1.1	0.2 ± 0.2
144	136 ± 19	38.7 ± 11.8	19.2 ± 3.8	11.7 ± 1.5	0.3 ± 0.1
			Control %ID/g		
4	4.1 ± 0.9	44.0 ± 11.3	86.4 ± 10.1	6.7 ± 0.9	1.8 ± 0.4
24	1.9 ± 0.3	33.9 ± 8.8	69.0 ± 3.2	11.9 ± 0.8	0.6 ± 0.1

1 lungs was approximately 30 times higher than that initially observed in the lungs of the control mice. Accumulation of radioisotope in the other organs of the group 1 mice (table 1, upper panel) was significantly lower than that observed in the lungs and was comparable to or lower than the comparable organs in group 2 animals. Comparison of group 2 lung accumulation with that in other major organs indicates that untargeted NP–mAb conjugates distributed mainly to liver and spleen in control mice. Bare particles (also) distribute mainly to the liver and spleen (supplementary figure 3, available at stacks.iop.org/Nano/18/175103).

Group 1 mice experienced a dramatic increase in spleen and liver accumulation after 1 h. We hypothesize two possible reasons why this may occur: first, the ratio of nanoparticles to antibody within each NP–mAb conjugate is variable, and some antibodies may not be completely effective depending on where the nanoparticle attaches and how many attach. Even pure antibodies are not completely effective, and exhibit a half-life at the target after which they are metabolized or otherwise removed. Likewise, there can be some cross-linking between multiple antibodies and nanoparticles. This hypothesis is supported by the TEM imaging of identically synthesized, non-radioactive samples of the same material. In the TEM images, some antibodies appear to be conjugated to as many as four nanoparticles (supplementary figure 1, available at stacks.iop.org/Nano/18/175103), and there was some aggregation noted. The aggregates are limited in size because we only selected a particular fraction for study (1–5 × 10^6 Da). This added mass and cross section probably shortens the antibody half-life *in vivo*. This may explain, as shown in table 1, the initial rapid drop in radioactivity from the lung and rapid increase in radioactivity in the spleen and liver. Hypothetically, the residual radioactivity in the lung comprises NPs that were bound to more optimum sites on the antibody, or were bound to antibodies with fewer other nanoparticles placing less stress on the antibody. For reference, the half-life of this antibody with no conjugated nanoparticles is approximately 6 days in the lung. The second hypothesis is a degradation of the bond between the nanoparticles and the antibody [17]. In order to test this hypothesis we ran two samples of the radioactive NP–mAb conjugates on SDS-PAGE (supplementary figure 2, available at stacks.iop.org/Nano/18/175103). The first sample was reduced with mercaptoethanol while the second was not. The antibody is labelled ^{125}I in these experiments, and only the nanoparticle

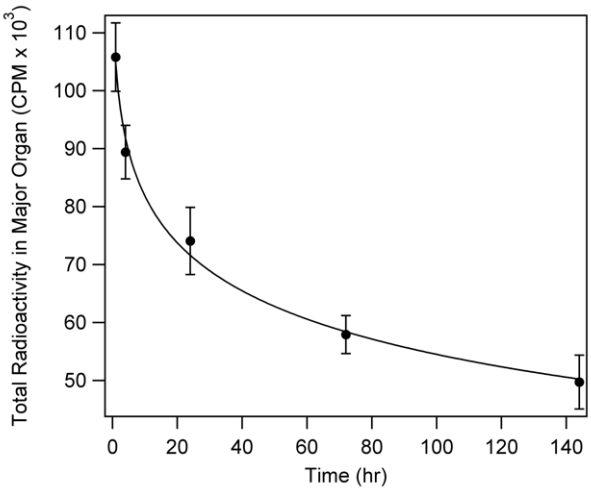

Figure 2. Whole body counts per minute (cpm) of major organs of group 1 mice. The decrease in total cpm was a function of internal redistribution of NP–mAb conjugates post-injection and NP–mAb clearance from the body. The clearance was fitted with a standard four-variable Hill equation. The rate of clearance from the body is approximately half that of the rate of clearance from the lung.

is unlabelled. The reduction separates the antibody into heavy and light fragment chains. Gamma radiation at the approximate masses for heavy and light chains reflects chains that were not bound to a nanoparticle, while gamma radiation at high mass (top of gel) is indicative of antibody fragments that are still bound to the immobile nanoparticle. Those antibody chains are still attached to the nanoparticle, even after exposure to a reducing environment. Clearly, the reduction that takes place between disulfide bonds of the antibody does not take place at the NP–mAb interface. In the light of this, we must conclude that the bond between the antibody and the nanoparticle is reasonably stable under these *in vitro* conditions.

All major organs except the kidneys in group 2 mice exhibited a decrease in radioactivity between 4 and 24 h post-injection. The kidneys typically participate in the removal of small molecules from the bloodstream, and the non-targeting NP–mAb conjugates used in the control mice were also susceptible to filtration by the kidneys. Rapid accumulation that occurs post-injection in the liver and spleen is probably caused by sequestration of the NP–mAbs by the reticuloendothelial system in the spleen and liver.

The estimate of overall rate of clearance of the NP–mAb conjugates from the group 1 mice is shown in figure 2. Total body radioactivity was estimated by addition of the collected organs using an estimate of 1.6 ml of blood per animal (8% of the body weight). The values are underestimated by the amount of material in non-collected organs; however, in this targeting system, a large fraction (85%) of the total injected radioisotope is recovered in lung, spleen, liver and kidneys. At 144 h the residual radioactivity in the lung had levelled off, yet the whole body radioactivity continued to drop, which is interpreted as the mouse clearing NP–mAb conjugates from the other major organs. The lung accumulation and whole body data were fitted with a standard four-variable Hill equation in order to assess the clearance rate and final lung and major organ concentrations of the NP–mAb conjugates. The Hill equation is often used to model protein-binding interactions and pharmaceutical dose-dependent effects [18]. In this application it is used to fit the rate of decrease of antibody in the lung. The rate of decrease in %ID/g in the lung was 0.66 h^{-1}, approximately twice the rate of decrease in %ID/g for all major organs (0.36 h^{-1}). The fits predict that the final radioactivity in the lung will be 125%ID/g. Experimentally the final radioactivity should eventually approach zero. The Hill fit for the whole body radioactivity (cpm) did eventually extrapolate to zero but at a time likely to be longer than the mouse lifespan. Hence, in order to assess the true long-term fate of the NPs *in vivo*, long-term biodistribution studies will be initiated.

In vivo SPECT/CT imaging experiments were carried out in order to visualize the biodistribution of the targeted and control NP–mAb and to demonstrate the potential for a nanoparticle-based radioimaging methodology. Mouse 1 was injected with NP coupled to control antibody and mouse 2 received ZnS/Cd^{125m}Te NP targeted with mAb 201B. Both mice were scanned on a Siemens dual-modality SPECT/MicroCAT II scanner originally optimized for ^{99m}Tc (see methods). The results of the scans (figure 3) clearly verify the biodistribution results reported in table 1. Mouse 1 (control, figure 3 bottom panel) shows significant accumulation of NP in the spleen and liver, but little detectable radioisotope binding in the lung cavity. In contrast, mouse 2 (figure 3, top panel), injected with NP targeted with mAb 201B shows accumulation primarily in the lung, with relatively little activity observed in the liver and spleen. While the images presented here are not quantitative, they provide indisputable proof that mAb conjugation can be used to effectively target NPs to specific anatomical sites with little non-specific accumulation within other regions of the body. Fully reconstructed models are provided as videos in the online multimedia files (available at stacks.iop.org/Nano/18/175103).

The use of a radioactive metal within a NP also affords an opportunity to observe the chemical stability of the NP in an aqueous environment. It is well known that semiconducting NPs such as CdSe and CdTe lose some optical fluorescence capacity after reaction with coordinating ligands. We reacted Cd^{125m}Te cores, without ZnS caps, with mercaptoacetic acid and suspended them in PBS. After 3 days at room temperature, approximately half of the radioactivity was released into solution, presumably as TeO_2^{2-} [19]. However, those same cores, when capped with ZnS, retained at least 97% of the

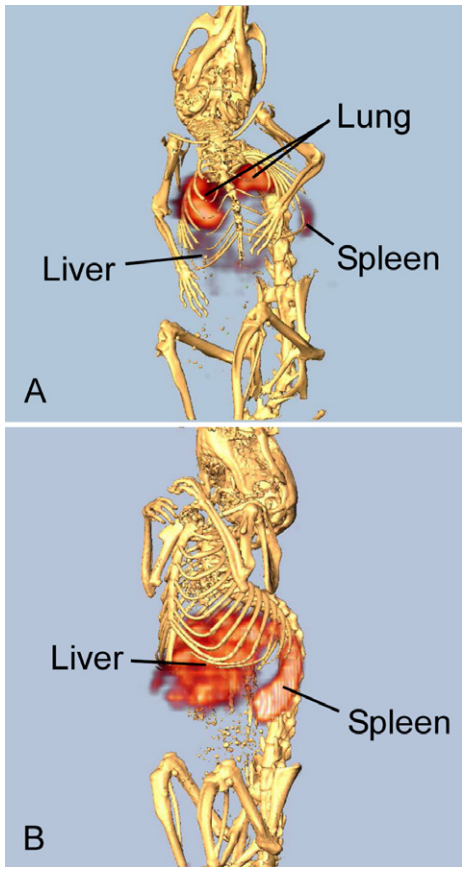

Figure 3. Whole body images of mouse 2 (A) and mouse 1 (B). Mouse 2 clearly shows accumulation of Cd^{125m}Te/ZnS–mAb in the left and right lobes of the lung, with some accumulation in the liver (large mass under lungs, left) and the spleen (right). Mouse 1 shows accumulation only in the liver and spleen. Mouse 1 nanoparticles were targeted with non-specific mAb 33.

radioactivity over a period of 1 week. A more rigorous experiment utilizing capped NP bound to antibody was performed for 1 month. For a series of three samples, at days 5, 9, 12 and 36, the average retained radioactivity was 96%, 92%, 91% and 90%. Clearly, the chemical stability of Cd^{125m}Te in an aqueous environment was enhanced by the ZnS shell. No effort was made to assess the toxicity of these nanoparticles in this experiment; however, since the nanoparticles are not appreciably soluble in the period of this experiment we expected, and observed, no toxicity to the mice. Also, the injected cadmium is two orders of magnitude below the LD/50 reported for cadmium in rat [20].

In summary, this work reports the synthesis of low-energy gamma-emitting, Cd^{125m}Te/ZnS NPs. The NPs were coupled to lung-targeting mAbs, tested *in vivo*, and found to accumulate selectively in lung tissue as measured by the emissions from the ^{125m}Te. SPECT/CT imaging of these same particles demonstrated the potential for use in medical imaging. These data suggest that by selection of radioisotopes with specific emission and chemical properties a potentially novel drug delivery system could be constructed. Radioactive NP–mAb conjugates may find applications in radioimmunotherapy as well as in medical diagnostic imaging.

Acknowledgments

Research sponsored by the Laboratory Directed Research and Development Program of Oak Ridge National Laboratory (ORNL) and the DOE Office of Biological and Environmental Research (OBER). ORNL is managed by UT-Battelle, LLC for the US Department of Energy under contract no. DE-AC05-00OR22725. The isotope Te-125*m* was produced at ORNL High Flux Isotope Reactor.

© notice. The submitted manuscript has been authored by a contractor of the US Government under contract no. DE-AC05-00OR22725. Accordingly, the US Government retains a nonexclusive, royalty-free license to publish or reproduce the published form of this contribution, or allow others to do so, for US Government purposes.

References

[1] Chan W C W and Nie S M 1998 Quantum dot bioconjugates for ultrasensitive nonisotopic detection *Science* **281** 2016–8

[2] Wang S P, Mamedova N, Kotov N A, Chen W and Studer J 2002 Antigen/antibody immunocomplex from CdTe nanoparticle bioconjugates *Nano Lett.* **2** 817–22

[3] Frey A *et al* 1999 Immunization of mice with peptomers covalently coupled to aluminum oxide nanoparticles *Vaccine* **17** 3007–9

[4] Tiefenauer L X, Kuhne G and Andres R Y 1993 Antibody magnetite nanoparticles—*in vitro* characterization of a potential tumor-specific contrast agent for magnetic-resonance-imaging *Bioconjug. Chem.* **4** 347–52

[5] Akerman M E, Chan W C W, Laakkonen P, Bhatia S N and Ruoslahti E 2002 Nanocrystal targeting *in vivo Proc. Natl Acad. Sci. USA* **99** 12617–21

[6] Gao X H, Cui Y Y, Levenson R M, Chung L W K and Nie S M 2004 *In vivo* cancer targeting and imaging with semiconductor quantum dots *Nat. Biotechnol.* **22** 969–76

[7] Bruchez M, Moronne M, Gin P, Weiss S and Alivisatos A P 1998 Semiconductor nanocrystals as fluorescent biological labels *Science* **281** 2013–6

[8] Goldenberg D M 2002 Targeted therapy of cancer with radiolabelled antibodies *J. Nucl. Med.* **43** 693–713

[9] McDevitt M R *et al* 2001 Tumor therapy with targeted atomic nanogenerators *Science* **294** 1537–40

[10] Milenic D E *et al* 2005 Alpha-particle radioimmunotherapy of disseminated peritoneal disease using a Pb-212-labelled radioimmunoconjugate targeting HER2 *Cancer Biother. Radiopharm.* **20** 557–68

[11] Kennel S J *et al* 2000 Evaluation of Ac-225 for vascular targeted radioimmunotherapy of lung tumors *Cancer Biother. Radiopharm.* **15** 235–44

[12] Mirzadeh S, Kumar K and Gansow O A 1993 The chemical fate of Bi-212-Dota formed by beta-decay of Pb-212(Dota)2 *Radiochim. Acta* **60** 1–10

[13] Kennel S J, Boll R, Stabin M, Schuller H M and Mirzadeh S 1999 Radioimmunotherapy of micrometastases in lung with vascular targeted Bi-213 *Brit. J. Cancer* **80** 175–84

[14] Peng Z A and Peng X G 2001 Formation of high-quality CdTe, CdSe, and CdS nanocrystals using CdO as precursor *J. Am. Chem. Soc.* **123** 183–4

[15] Kennel S J, Lankford T, Hughes B and Hotchkiss J A 1988 Quantitation of a murine lung endothelial-cell protein, P112, with a double monoclonal-antibody assay *Lab. Invest.* **59** 692–701

[16] Ford V A, Stringer C and Kennel S J 1992 Thrombomodulin is preferentially expressed in Balb-C lung microvessels *J. Biol. Chem.* **267** 5446–50

[17] Kulkarni S K *et al* 2001 Investigations on chemically capped CdS, ZnS and ZnCdS nanoparticles *Appl. Surf. Sci.* **169/170** 438–46

[18] Giraldo J, Vivas N M, Vila E and Badia A 2002 Assessing the (a)symmetry of concentration–effect curves: empirical versus mechanistic models *Pharmacol. Ther.* **95** 21–45

[19] Fritsche J *et al* 2001 Surface analysis of CdTe thin film solar cells *Thin Solid Films* **387** 161–4

[20] Leber A P and Miya T S 1976 A mechanism for cadmium- and zinc-induced tolerance to cadmium toxicity: involvement of metallothionein *Toxicol. Appl. Pharmacol.* **37** 414